Sampling-Distribution-Based Evaluation for Monte Carlo Rendering

Christian Freude[a], Hiroyuki Sakai[b], Károly Zsolnai-Fehér[c] and Michael Wimmer[d]
Institute of Visual Computing and Human-Centered Technology, TU Wien, Favoritenstr. 9-11 / E193-02, Vienna, Austria

Keywords: Computer Graphics, Rendering, Ray Tracing, Evaluation, Validation.

Abstract: In this paper, we investigate the application of per-pixel difference metrics for evaluating Monte Carlo (MC) rendering techniques. In particular, we propose to take the sampling distribution of the mean (SDM) into account for this purpose. We establish the theoretical background and analyze other per-pixel difference metrics, such as the absolute deviation (AD) and the mean squared error (MSE) in relation to the SDM. Based on insights from this analysis, we propose a new, alternative, and particularly easy-to-use approach, which builds on the SDM and facilitates meaningful comparisons of MC rendering techniques on a per-pixel basis. In order to demonstrate the usefulness of our approach, we compare it to commonly used metrics based on a variety of images computed with different rendering techniques. Our evaluation reveals limitations of commonly used metrics, in particular regarding the detection of differences between renderings that might be difficult to detect otherwise—this circumstance is particularly apparent in comparison to the MSE calculated for each pixel. Our results indicate the potential of SDM-based approaches to reveal differences between MC renderers that might be caused by conceptual or implementation-related issues. Thus, we understand our approach as a way to facilitate the development and evaluation of rendering techniques.

1 INTRODUCTION

Simulating light transport for the synthesis of photorealistic images is of great importance for film production, architectural visualization, product design, and many other applications. Predominant approaches to solve this problem are based on a model described by the *rendering equation* (Kajiya, 1986) and evaluate its numerous integrals using Monte Carlo (MC) integration.

This type of integration approximates the integral of a function through exhaustive random sampling. Due to the stochastic nature of this approach, the approximations generally suffer from variance, which manifests itself as noise in the rendered images. As the number of samples increases, the variance eventually vanishes and the integral converges to the correct solution.

A significant amount of research has been dedicated to reduce variance and speed up convergence by using more advanced sampling strategies. However, the variance inherent to all MC-based rendering techniques impedes their comparison, as images are only completely noise-free in the *theoretical* limit, which generally cannot be attained in practice. Moreover, commonly used difference metrics do not take this variance fully into account.

In this paper, we investigate the potential of sampling distribution-based approaches for the comparison and evaluation of MC renderings and techniques on a per-pixel basis. The key insight is that conventional metrics, such as the absolute deviation (AD) or mean squared error (MSE), only incorporate limited information about the distributions of per-pixel radiance estimates. We see great potential in incorporating additional information, in particular information about the sampling distribution of the mean (SDM), to develop improved measures that can reveal differences more clearly than other approaches. The underlying intuition is that the SDM includes information about the variability of per-pixel radiance estimates at a particular stage of convergence, i.e., for a particular number of samples per pixel (SPP). Therefore, the accuracy of the renderings can be incorporated into the measure and leveraged for comparison.

We propose a novel, alternative approach that builds on the estimation of the SDM. It essentially estimates the probability that one integrator produces similar radiance estimates as another. Our approach can be used for effectively comparing and evaluating

[a] https://orcid.org/0000-0002-4224-4105
[b] https://orcid.org/0000-0003-0388-8458
[c] https://orcid.org/0000-0003-3707-6319
[d] https://orcid.org/0000-0002-9370-2663

Freude, C., Sakai, H., Zsolnai-Fehér, K. and Wimmer, M.
Sampling-Distribution-Based Evaluation for Monte Carlo Rendering.
DOI: 10.5220/0011886300003417
In *Proceedings of the 18th International Joint Conference on Computer Vision, Imaging and Computer Graphics Theory and Applications (VISIGRAPP 2023) - Volume 1: GRAPP*, pages 119-130
ISBN: 978-989-758-634-7; ISSN: 2184-4321

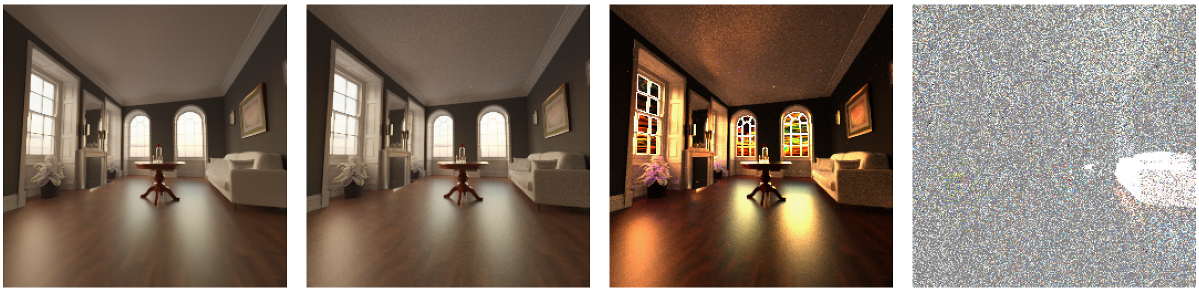

(a) Unbiased Reference (b) Biased Rendering (c) Per-Pixel Root Mean Squared Error (d) Our Approach for Evaluation

Figure 1: Here, we illustrate the potential of our proposed approach for the evaluation of Monte Carlo (MC) rendering techniques. It is based on the sampling distribution of the mean (SDM). Image (a) shows a reference rendering and (b) an artificially biased rendering for which the reflectance of the couch on the right-hand side was reduced. Our approach (d) can reveal differences between both renderings that are difficult to identify through visual comparison or other metrics, e.g., the (normalized) root mean squared error (RMSE) calculated for each pixel (c). This circumstance suggests the viability of using SDM-based approaches for the per-pixel comparison of MC renderings.

MC renderings and techniques (see Figure 1).

The closely related work by Jung et al. (Jung et al., 2020) already demonstrated how statistical approaches can be used effectively to reveal bias in rendered images. They show that a non-uniform distribution of p-values (based on the Welch's test statistic) is an indicator for bias. In contrast, we compute the probability that one renderer computes similar radiance values as another and moreover facilitate meaningful comparisons between unbiased integrators. We see our approach as an alternative to the work by Jung et al.

The remainder of our paper is structured as follows: In Section 2, we provide an overview over related work. To motivate the incorporation of additional statistical information, such as the SDM, we discuss the statistical background and provide a theoretical comparison of different measures in Section 3. In Section 4, we present our approach. Furthermore, in Section 5, we evaluate the measures based on renderings of several scenes computed by different integrators. Our examples illustrate how well the measures are able to reveal differences between renderings. We show that sampling-distribution-based measures are consistently able to reveal subtle differences. Moreover, we point out shortcomings of per-pixel mean squared error (ppMSE) in particular.

2 RELATED WORK

In previous work, researchers proposed various methods for the comparison and evaluation of Monte Carlo (MC) renderings. In the following, we provide an overview over those methods.

Perceptual Metrics. Many researchers employed a perceptual model that can be used to approximate perceived differences, which in turn can be exploited for rendering. For instance, the visible differences predictor (Daly, 1993) has been employed to approximate perceived rendering quality in order to use it for a stopping condition (Myszkowski, 1998) or to alternate between complementary rendering techniques (Volevich et al., 2000). Ramasubramanian et al. (Ramasubramanian et al., 1999) developed a perceptual error metric for image-space adaptive sampling. Farrugia and Péroche (Farrugia and Péroche, 2004) used an existing vision model (Pattanaik et al., 1998) in order to achieve the same goal. Andersson et al. (Andersson et al., 2020) presented an approach that can estimate the perceived difference while alternating between two images. In contrast, we focus on the direct comparison of radiance estimates, as we strive for objective and quantitative assessments for MC rendering.

General Image Quality Metrics. Most researchers leveraged general image quality metrics, which are popular in the image-processing community, to compare MC renderings. Prominent examples are the mean squared error (MSE), the root mean squared error (RMSE), peak signal-to-noise ratio (PSNR), the structural similarity (SSIM) index (Wang et al., 2004), and variants of the high-dynamic-range visual difference predictor (HDR-VDP) (Mantiuk et al., 2005; Mantiuk et al., 2011; Narwaria et al., 2015). For instance, Meneghel and Netto (Meneghel and Netto, 2015) employed SSIM and HDR-VDP2 for the comparison of six different rendering techniques.

Whittle et al. (Whittle et al., 2017) provided a comprehensive overview and analysis of a multitude of general image quality metrics. The problem with such *general* metrics is that they are agnostic to the sample distributions in MC rendering, which can potentially provide a breadth of additional information. By incorporating information about distributions, we strive to provide a better alternative to those metrics.

Rendering Verification. Several works (Goral et al., 1984; McNamara et al., 2000; Schregle and Wienold, 2004; Meseth et al., 2006; McNamara, 2006; Bärz et al., 2010; Jones and Reinhart, 2017; Clausen et al., 2018) compare renderings to real-world measurements in order to assess rendering quality. Ulbricht et al. (Ulbricht et al., 2006) investigated the state of the art for the verification of renderings and pointed out that all approaches have their weaknesses and that the development of robust and practical solutions is still an open task. Nevertheless, the verification of rendering techniques using real-world measurements is orthogonal to our goal of comparing different rendering techniques.

Statistical Approaches. Compared to the methods discussed so far, statistical approaches are most relevant to ours. Celarek et al. (Celarek et al., 2019) proposed an approach to estimate MSE expectation and variance and to analyze the error distribution over frequencies of MC rendering techniques. Subr and Arvo (Subr and Arvo, 2007) employed statistical tests to compare rendering techniques. However, they used test hypotheses that are not suited to test for equality but can only show significant differences. The method by Jung et al. (Jung et al., 2020) also builds on classical hypothesis testing—specifically, Welch's test—by considering non-uniform distributions of p-values as indicators for bias. Welch's test also incorporates more information about sampling distributions, which makes it comparable to our proposed approach. However, our approach is not based on p-values but computes probabilities that one renderer produces radiance estimates similar as another. Furthermore, it can also be used to compare unbiased renderers. In Section 5, we discuss the differences between the approach by Jung et al. and ours in more detail.

In general, there has been a surprisingly low amount of research on statistical approaches to compare MC renderings and rendering techniques. Thus, with our approach, we aim not only to provide a novel, useful alternative to existing approaches but also to inspire further research in this direction.

3 BACKGROUND

In this section, we describe the theoretical background and analyze common difference metrics in relation to the sampling distribution of the mean (SDM) in order to motivate the use of the latter for the evaluation of Monte Carlo (MC) renderings. Moreover, we discuss the closely related approach by Jung et al. (Jung et al., 2020).

3.1 Prerequisites

A MC rendering technique generates an image by evaluating the rendering equation for each pixel by means of MC integration. Due to the nature of this approach, it can only *estimate* the involved integrals, which generally leads to noise in the rendered image. Typically, to assess quality and performance, a noiseless *reference* is computed against which the rendered image can be compared. Such a reference generally requires a very high sample budget to ensure that its error is relatively low. The difference between the rendered image to its reference is then quantified using metrics like absolute deviation (AD), mean squared error (MSE), or some variant thereof, either aggregated over the whole image or per pixel.

Aggregate vs. Per-Pixel Metrics. Usually, metrics such as the AD or MSE are computed incorporating all pixels to form a single scalar difference value for an individual image with respect to a reference. This approach is useful when images need to be compared on the basis of a single aggregated value, but it does not help to identify the locations where the images are different. This can rather be achieved by using per-pixel difference metrics.

In this work, we focus on the per-pixel comparison of MC renderings; thus, if not stated otherwise, all metrics in our exposition are applied on a per-pixel basis. One fundamental shortcoming of applying commonly used metrics per pixel is that they do not take the accuracy or state of convergence of the renderings into account. In the following, we illustrate this issue and propose a potential solution based on the SDM, which we first review in the next paragraphs.

Sampling Distribution of the Mean. The samples computed by a MC integrator for a particular pixel can be seen as a random variable X from an arbitrary distribution f_X with an unknown population mean μ_X and variance σ_X^2. The distribution mainly depends on the type of the integrator and the scene. During rendering, an increasing number of samples from this

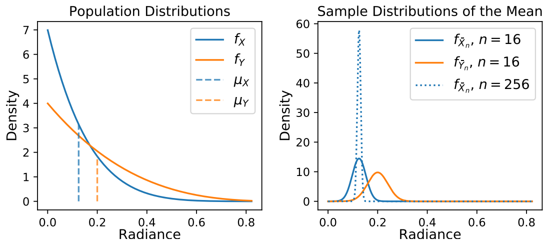

Figure 2: These plots show the relation between the population distributions (left) and the sampling distributions of the mean (SDMs) (right) of two random variables X (blue) and Y (orange) representing pixel radiance samples computed by two integrators. (For this illustration, we have used two beta distributions for X and Y that differ slightly in mean and variance.) According to the CLT (Equation 1), the SDM approaches normality and decreases in standard deviation (SD) as sample size n increases (right; dotted blue line).

distribution are averaged to estimate μ_X, i.e., by computing the sample mean $\bar{X}_n$ using n samples per pixel (SPP).

In contrast to f_X, the sampling distribution of the mean (SDM) $f_{\bar{X}_n}$ not only depends on μ_X and σ_X^2 but also on the sample size n; the central limit theorem (CLT) states that the SDM is approximately normal-distributed for a sufficiently large n:

$$\bar{X}_n \sim \mathcal{N}\left(\mu_X, \frac{\sigma_X}{\sqrt{n}}\right). \tag{1}$$

Furthermore, the standard deviation (SD) of the SDM $\sigma_{\bar{X}_n} = \sigma_X/\sqrt{n}$ is known as the standard error of the mean (SEM), which can be used to quantify the error of a MC rendering. This error is proportional to σ_X, i.e., the SD of the integrator, and inversely proportional to n. These relationships are consistent with the fact that error can be reduced by decreasing the SD of the integrator σ_X or increasing the number of samples n.

3.2 Issues of Commonly Used Metrics

In this section, we aim to clarify the shortcomings of commonly used metrics such as the AD and MSE. To this end, Figure 2 illustrates the relation between the population distribution and the SDM. Here, random variables X (blue) and Y (orange) represent pixel radiance samples computed by two integrators. Averaging transforms their population distributions (left) into their corresponding SDMs (right). We note that the means and therefore the bias remain unchanged. For the same sample size $n = 16$, the SEMs $\sigma_{\bar{X}_n}$ and $\sigma_{\bar{Y}_n}$ are proportional to the SDs of the corresponding population distributions (both scaled by a factor of $1/4$). As we increase the sample size from 16 to 256 for the sample mean $\bar{X}_n$ (which we hereafter consider as the reference), the SEM $\sigma_{\bar{X}_n}$ decreases (dotted blue line). Therefore, the SDM inherently includes information about the error for different states of convergence.

With these considerations in mind, we now focus on two commonly used metrics. The AD only evaluates $|\mu_X - \mu_Y|$, i.e., the difference between means (known as bias), and therefore does not include any information about the SDM. The MSE can be written as the sum of variance and squared bias:

$$\begin{aligned}
\mathrm{MSE}(\hat{\theta}, \theta) &= \mathbb{E}\left(\left(\hat{\theta} - \theta\right)^2\right) \\
&= \mathbb{E}(\hat{\theta}^2) + \mathbb{E}(\theta^2) - 2\theta\mathbb{E}(\hat{\theta}) \\
&= \mathbb{E}(\hat{\theta}^2) \underbrace{- \mathbb{E}^2(\hat{\theta}) + \mathbb{E}^2(\hat{\theta})}_{=0} + \mathbb{E}(\theta^2) - 2\theta\mathbb{E}(\hat{\theta}) \\
&= \mathrm{Var}(\hat{\theta}) + \mathbb{E}^2(\hat{\theta}) + \theta^2 - 2\theta\mathbb{E}(\hat{\theta}) \\
&= \mathrm{Var}(\hat{\theta}) + \left(\mathbb{E}(\hat{\theta}) - \theta\right)^2 \\
&= \mathrm{Var}(\hat{\theta}) + \mathrm{Bias}(\hat{\theta}, \theta)^2
\end{aligned} \tag{2}$$

where $\hat{\theta}$ is the estimator and θ is the parameter being estimated.

Equation 2 reveals a potential shortcoming of the MSE: one can exchange variance for bias (and vice versa) without changing the result. Another problem is that the MSE assumes knowledge about the parameter being estimated—in our case, the population mean $\theta = \mu_X$ of the reference. In general, the population mean is unknown and must be estimated, but the distribution of this estimate (the SDM) cannot be taken into account in the MSE. Only the distribution of the estimate $\hat{\theta} = \bar{Y}_n$ is accounted for:

$$\mathrm{MSE}(\bar{Y}_n, \mu_X) = \mathrm{Var}(\bar{Y}_n) + \mathrm{Bias}(\bar{Y}_n, \mu_X)^2. \tag{3}$$

Aggregate vs. Per-Pixel MSE. We also want to point out the key difference between applying the MSE across all pixels of the image and applying it per pixel. The former computes the mean squared difference between corresponding pixels of two images and therefore tends toward zero as the difference between those images decreases. The latter computes the mean squared difference between random samples and a fixed reference value for each individual pixel. Therefore, the per-pixel MSE (ppMSE) converges to the variance plus squared bias of the used MC integrator. This property makes the ppMSE less suited for the comparison of MC renderings, as we illustrate with the results shown in Section 5.1.

Apart from the issues mentioned so far, both AD and MSE do not include the additional information provided by the SDM or SEM, in particular, the accuracy or state of convergence of the estimates at a specific sample size n. This circumstance is shown

Table 1: An overview of the types of information that are considered by various difference measures (including ours). Bias is considered by all measures. The MSE additionally incorporates the variance of the non-reference distribution. Our approach, as well as the one by Jung et al. (Jung et al., 2020), moreover takes the variance of the reference distribution and, more importantly, the SDMs into account.

	Bias	**Variance (non-ref.)**	**Variance (reference)**	**Sample Distr. of the Mean**
AD	✔	✘	✘	✘
MSE	✔	✔	✘	✘
(Jung et al., 2020)	✔	✔	✔	✔
SDMP (Ours)	✔	✔	✔	✔

in Table 1. It includes our proposed measure, which additionally incorporates the error of the reference, but more importantly, is based on estimations of the SDM to take the SEM into account. The information that we additionally take into account can facilitate the evaluation and comparison of different MC renderings and techniques, as evidenced by the results shown in Section 5. In addition to the metrics discussed in this section, Table 1 also includes an approach recently published by Jung et al. (Jung et al., 2020), which we discuss in the next section.

3.3 The Approach by Jung et al.

The approach by Jung et al. (Jung et al., 2020) is based on hypothesis testing and provides a similar feature set as our method. It is based on Welch's two-sample test for the difference in means. Specifically, they compute p-values for image tiles and analyze their distribution. They have shown that a non-uniform distribution of p-values is an indicator for bias, as under the null hypothesis (i.e., no bias), the p-values are expected to be uniformly distributed. By using MC samples averaged over tiles, they facilitate the normality of the sample means, which is required for Welch's test.

Intuitively, a lower p-value indicates a higher probability of the (population) means being different. If the p-value is less than or equal to the specified significance level α, the difference between means is considered significant. But this only suggests a difference and cannot show equivalence. Nevertheless, Jung et al. have shown that visualizing p-values per tile can give clues about biased regions and that a uniform distribution of p-values indicates the absence of bias. The similarities and differences between theirs and our approach are discussed in Section 5, where we also provide examples that demonstrate the advantages of our approach.

4 OUR APPROACH

In the previous section, we described how the SDM incorporates useful information about the rendering process that is missing in classical metrics. Thus, we propose to use the SDM for quantifying the similarity between the radiance estimates produced by different MC integrators. Our idea is to, for each pixel, estimate the SDM and compute the probability that the corresponding radiance estimates are similar to the one produced by another integrator. In the following, we derive the formulas for calculating this probability.

Probability of the Sample Mean $\bar{X}_n$. We first consider a single integrator and determine the probability that it generates sample mean values, represented by a random variable $\bar{X}_n$, in a certain range for a particular pixel. The corresponding SDM $f_{\bar{X}_n}$ is defined in Equation 1. Since the probability of $\bar{X}_n$ taking on any particular value in a continuous space is zero, we can only derive probabilities for intervals $(a_{\bar{X}_n}, b_{\bar{X}_n}]$. Given the cumulative distribution function (CDF) $F_{\bar{X}_n}$ corresponding to $f_{\bar{X}_n}$, the probability that the integrator produces radiance estimates in a certain interval $(a_{\bar{X}_n}, b_{\bar{X}_n}]$ can be derived as follows:

$$
\begin{aligned}
P(a_{\bar{X}_n} < \bar{X}_n \leq b_{\bar{X}_n}) &= P(\bar{X}_n \leq b_{\bar{X}_n}) - P(\bar{X}_n \leq a_{\bar{X}_n}) \\
&= F_{\bar{X}_n}(b_{\bar{X}_n}) - F_{\bar{X}_n}(a_{\bar{X}_n})
\end{aligned} \tag{4}
$$

Furthermore, we consider the inverse CDF or quantile function $Q_{\bar{X}_n} = F_{\bar{X}_n}^{-1}$, which can be used to find an interval that contains a certain probability mass of the distribution. In particular, we are interested in the interval whose endpoints are equidistant to the mean $\bar{X}_n$ and enclose the fraction $1-\alpha$ of all possible values:

$$
(a_{\bar{X}_n}, b_{\bar{X}_n}] = \left(Q_{\bar{X}_n}\left(\frac{\alpha}{2}\right), Q_{\bar{X}_n}\left(1-\frac{\alpha}{2}\right)\right]. \tag{5}
$$

This interval, which turns out to be the confidence interval (CI) for the sample mean, can be used to determine the probability that one integrator will produce similar radiance estimate as another, as we describe in the following.

Probability for Comparing Integrators. Our approach is to select one integrator (which generates samples X) and compute the CI for its estimates $(a_{\bar{X}_n}, b_{\bar{X}_n}]$ according to Equation 5. We further determine the probability that another integrator (which generates samples Y) produces estimates $\bar{Y}_n$ within this interval. Specifically, we compute how much probability mass of the SDM of Y lies inside the CI

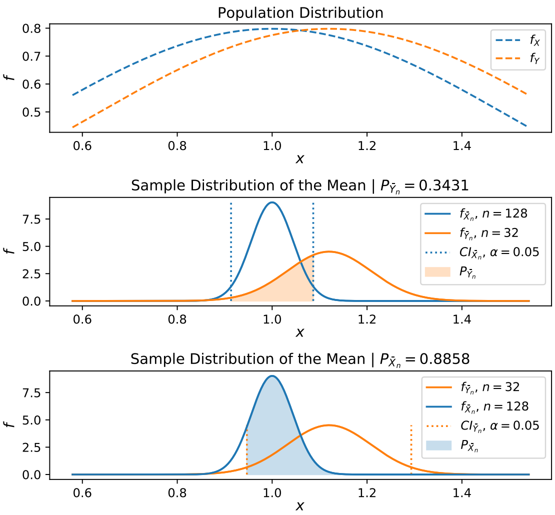

Figure 3: An illustration of the asymmetry of our approach. At the top, population distributions for X and Y are shown, which have equal σ but different μ. Below, corresponding SDMs for different sample sizes for $\bar{X}_n$ and $\bar{Y}_n$ are shown. Since the SDM of X has a lower SD than that of Y, the probabilities are not equal.

for the mean of X. This approach requires the integration of $f_{\bar{Y}_n}$ over the interval $(a_{\bar{X}_n}, b_{\bar{X}_n})$[1]:

$$\begin{aligned} P(a_{\bar{X}_n} < \bar{Y}_n \leq b_{\bar{X}_n}) &= \int_{a_{\bar{X}_n}}^{b_{\bar{X}_n}} f_{\bar{Y}_n}(x)dx \\ &= F_{\bar{Y}_n}(b_{\bar{X}_n}) - F_{\bar{Y}_n}(a_{\bar{X}_n}). \end{aligned} \tag{6}$$

This equation describes the probability that $\bar{Y}_n$ takes on values that fall into the CI for $\bar{X}_n$ at a confidence level $1-\alpha$. Thus, it can be used to quantify the similarity of the radiance estimates produced by two integrators.

We note that this probability is not symmetric: exchanging $\bar{X}_n$ and $\bar{Y}_n$ results in a different probability, as illustrated in Figure 3. Intuitively, our approach computes the overlap of one distribution with the CI of another, which is only symmetrical if $\sigma_{\bar{X}_n} = \sigma_{\bar{Y}_n}$.

We propose to choose $\bar{X}_n$ as the reference, for which the error is relatively low. In this case, if $\mu_Y = \mu_X$, the probability increases with the accuracy of $\bar{Y}_n$ as more of its probability mass falls into the CI of the reference.

The corresponding probability of dissimilarity is given by

$$1 - P(a_{\bar{X}_n} < \bar{Y}_n \leq b_{\bar{X}_n}). \tag{7}$$

For our evaluation in Section 5, we have used this dissimilarity, i.e., the probability that a *test* renderer computes sample means that fall outside the CI for the mean of a *reference* renderer. We hereafter refer to it as SDM-based probability (SDMP).

In cases where no reference is available, it may be desirable to compare renderings on equal ground, which would require a symmetric measure. A possible symmetric variant of our measure can be given by the average

$$\frac{2 - P(a_{\bar{X}_n} < \bar{Y}_n \leq b_{\bar{X}_n}) - P(a_{\bar{Y}_n} < \bar{X}_n \leq b_{\bar{Y}_n})}{2}. \tag{8}$$

Other operations such as the minimum or maximum of the two probabilities might also be of interest. In this work, we focus on our asymmetric measure for similarity and leave the investigation of symmetric variants for future work.

Practical Considerations. In practice, since population parameters are generally not available, our approach builds on sample estimates. Conveniently, the required estimates can be computed *online*, i.e., without the need to store individual samples (e.g., by using Welford's algorithm (Welford, 1962)). For integrators such as path tracing (PT), the estimates can be directly computed from individual radiance samples as long as the sample count is sufficient to assume normal distribution. In cases where the sample count is insufficient, we can effectively increase it by aggregating over multiple pixels, as proposed by Jung et al. (Jung et al., 2020). For more sophisticated integrators such as Metropolis light transport (MLT), we can average multiple estimates in form of *short renderings*, as suggested by Celarek et al. (Celarek et al., 2019).

The significance level α can be used to control the sensitivity of our approach, i.e., the length of the CI of $\bar{X}_n$ used for calculating the probability. Since the SD of the reference renderer can be estimated in advance, it is possible to choose the α in such a way that the CI corresponds to a desired range of radiance values.

5 EVALUATION

In this section, we first show how our approach compares to other metrics. Afterward, we discuss the closely related work by Jung et al. (Jung et al., 2020) to which we also refer as JHD20 for brevity.

5.1 General Comparison

In the following, we investigate different approaches for identifying differences in Monte Carlo (MC) renderings. In particular, we compare our approach to per-pixel absolute deviation (AD), root mean squared

[1] Here, for brevity, we use f to denote the probability density function (PDF) of the distribution instead of the distribution itself.

error (RMSE), and JHD20. (We choose RMSE instead of mean squared error (MSE) since it expresses the error in the same unit as the radiance values.)

We note that the comparisons provided in Figures 4 to 7 are structured similarly: In the first column, we show the renderings and in the second, the corresponding sample standard deviation (SD). The remaining columns show images of the different approaches. The rows correspond to independently computed renderings. The first row corresponds to the reference rendering (computed with a relatively high sample count) and the others correspond to test renderings (computed with a lower sample count). Specifically, the second row corresponds to an unbiased control rendering and the last row to an artificially biased rendering, for which a scene property has been slightly changed. For this artificial bias, we have kept the actual integrator implementation unmodified. Moreover, we provide the average value for each image (shown below the label). We note that in our figures, we show all non-radiance values as RGB images for compact display, instead of separately displaying the individual channels.

We have used 32 768 SPP to compute the reference renderings and 4096 SPP in all other cases (unless stated otherwise). The AD and RMSE values are bounded by $[0,\infty)$. The p-values computed by JHD20 fall between 0 and 0.5 on average. Our approach computes probabilities in the interval $(0,1)$. We note that in case of JHD20, low values indicate bias, while for the other approaches, high values indicate dissimilarity. We have used the scenes provided by Bitterli (Bitterli, 2016).

Living Room Scene. Figure 4 shows the results for the LIVING ROOM scene rendered using PT. For the unbiased control rendering (second row), the AD and the RMSE contain structures that can distract from identifying bias. In contrast, our SDM-based probability (SDMP) and JHD20 (last two columns) show no structure but homogeneous noise. We also illustrate this circumstance in Figure 8, which shows that in the frequency domain, the spectrum of both approaches is relatively uniform compared to the AD and RMSE.

We note that since the control rendering has no bias, the RMSE is essentially the same as the SD in this case. This circumstance stems from the bias–variance decomposition described in Equation 2. The only difference is that the RMSE uses the factor $1/n$ instead of $1/(n-1)$ for normalization.

For the biased rendering (third row), only our SDMP and JHD20 clearly reveal the bias caused by the sofa. In the case of the AD, the bias can be seen, especially in comparison to the control image, but it is accompanied by potentially distracting regions of structured noise. For the RMSE, the biased region cannot be visually discerned. These circumstances demonstrate how scene features and the SD of the integrator can manifest themselves as structures in the measures that can mask bias—a detriment that both our SDMP and JHD20 do not suffer from.

Veach Ajar Scene. Figure 5 shows the results for the VEACH AJAR scene rendered using BDPT. Here, we can see, similarly to the previous LIVING ROOM example in Figure 4, that our SDMP and JHD20 clearly reveals the bias caused by the floor, while the AD and RMSE are less effective in this regard due to additional potentially distracting structures.

For this scene, we also investigate the convergence of the different approaches with increasing SPP. In Figure 6, we can see how distracting scene structures are visible in all AD and RMSE images. In contrast, our SDMP and JHD20 show the bias (caused by the floor) more clearly.

In Figure 9, plots of the corresponding average image values with respect to the SPP are shown. We can see how the average RMSE matches the corresponding average SD, and that the average RMSE for the biased rendering is (counterintuitively) lower than for the control. This fact indicates that the RMSE is not well-suited to identify bias. In contrast, the average AD reveals the increase in error for the biased renderings and gets more accurate with increasing sample count. JHD20 is able to show bias; however, the average value in the control case stays constant, i.e., it does not show the increase in accuracy due to the increased sample count. In contrast, our SDMP indicates this increased accuracy for the control rendering, suggesting its use for the comparison of unbiased renderers.

Veach Bidir Room Scene. For the last comparison, we have chosen the VEACH BIDIR ROOM scene, shown in Figure 7. In this scene, the bias is caused by a change in intensity for the spotlight that illuminates the left-hand wall. It is imperceptible in the renderings as well as in the RMSE.

An interesting observation can be made by comparing the average values of the different measures (below the labels). The average RMSE would (counterintuitively) indicate that the biased rendering (last row) is closer to the reference. However, the other average values show that the unbiased rendering is indeed more accurate than the biased one, indicating that these measures are more suited for per-pixel comparison.

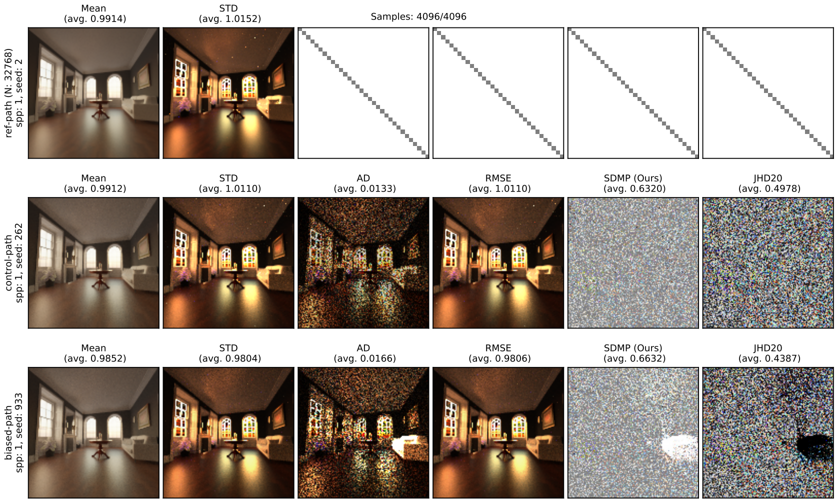

Figure 4: Renderings of the LIVING ROOM scene and the corresponding per-pixel images of different approaches for quantifying the difference between renderings. All three renderings (leftmost column) were computed using path tracing (PT). The bottom row shows an artificially biased version of the scene, for which the reflectance of the sofa on the right-hand side was reduced. The structure of the scene is visible in the AD and RMSE images. Our approach and JHD20 reveal the biased image region at the sofa (last row).

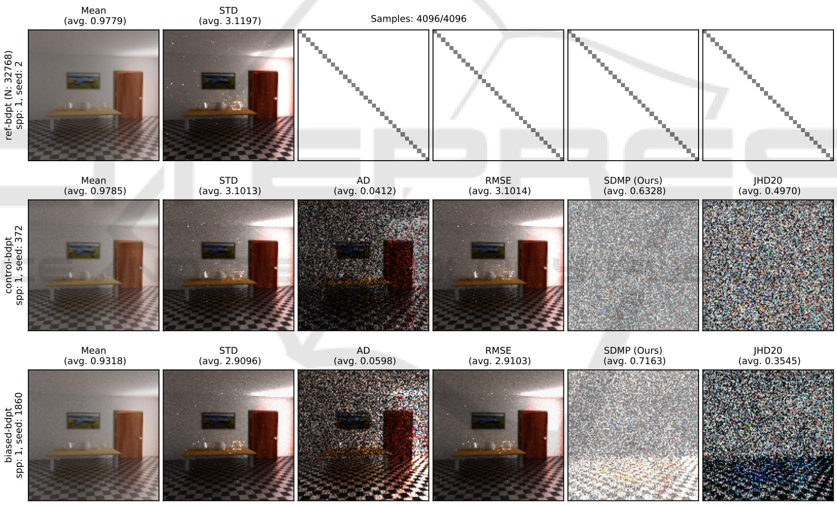

Figure 5: Renderings of the VEACH AJAR scene and the corresponding per-pixel images of different approaches for the comparison of renderings. All three renderings (leftmost column) were computed using bidirectional path tracing (BDPT). The third row shows an artificially biased version of the scene, for which the reflectance of the floor was reduced. The structure of the scene is still visible in comparison the AD and RMSE images, while our approach and JHD20 reveal the biased image region at the floor (last row).

Another observation is that in this scene, outliers due to fireflies are relatively frequent. Those additionally introduce distractions in the difference images. Moreover, they can transform the sample distributions such that the normality assumption—upon which SDMP and JHD20 rely—is violated. We illustrate this issue in Figure 13 and discuss it in the next section (5.2).

Application Scenarios. We see two main application scenarios for our approach: The first scenario is the per-pixel comparison to indicate similarity or bias in different regions of the image. The second scenario is the numerical comparison based on the average SDMP, either computed across the whole image or a region of interest.

Let us assume that we are interested in the difference between multiple renderings with respect to each other or to a reference. The magnitude of the SDMP image indicates the amount of difference. This difference can be visually inspected or compared numerically using values averaged over the whole or a par-

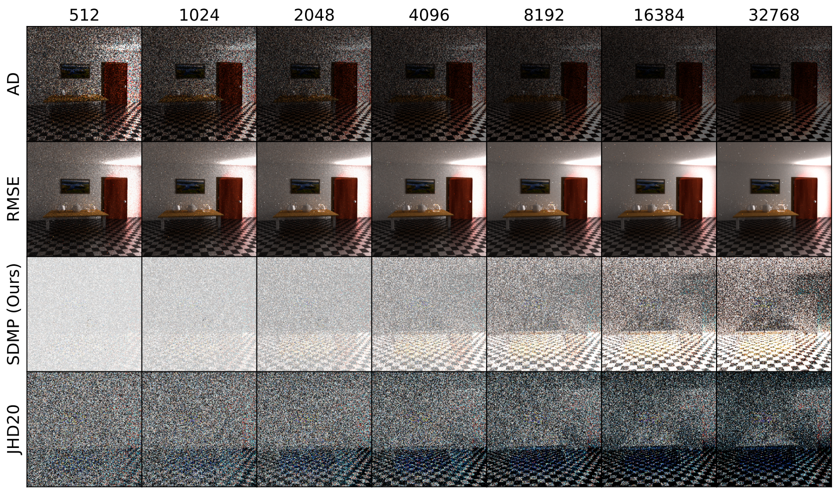

Figure 6: Images of different measures (rows) for increasing samples per pixel (SPP) (columns) for the biased variant of the VEACH AJAR scene. Here, we can see that the AD decreases while many regions, e.g. the back wall, remain noisy. By contrast, the noise in the RMSE images vanishes more quickly, while the images converges to the SD of the BDPT integrator. In comparison, our approach and JHD20 reveal the bias more clearly, since other scene features are less noticeable. The convergence of the corresponding average image values is illustrated in Figure 9.

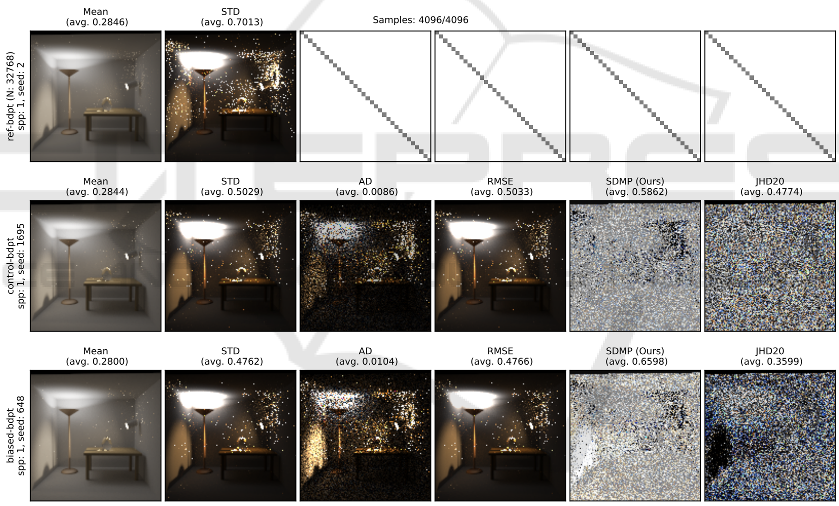

Figure 7: Comparison of measures based on the VEACH BIDIR ROOM scene. The biased variant (bottom row) was created by decreasing the emission of the spotlight mounted on the right-hand wall. All renderings were computed using BDPT. The introduced bias results in an increased intensity of the illumination on the left-hand wall. Here all approaches, except RMSE, are able to show the biased region; however, our approach and JHD20 exhibit less structure in other image regions.

ticular region of the image. We provide examples of such visual comparisons in Figures 4 to 6 and a basic example of numerical comparison in Figure 9.

Additional examples of numerical comparisons are provided in Figures 10 to 11. Here, we illustrate the properties of the SDMP in comparison to the other measures based on the VEACH AJAR scene. We compare average values of the measures with respect to sample count. These average values are computed across the top image region, the bottom region, and the full image, as illustrated in Figure 12. For the unbiased control rendering (Figure 10), AD and RMSE exhibit different average values for each region. Our SDMP and JHD20 exhibit the same average values for all regions. This is due to their beneficial uniform spectrum, as shown in Figure 8.

Furthermore, it can be seen that the SDMP assigned a lower value (less difference) for the low-quality reference case (dashed lines). This is because the confidence interval (CI) for the low-quality reference is much broader than the CI of the high-quality reference and therefore includes more probability mass of the sampling distribution of the mean (SDM) of the test rendering. This shows that our ap-

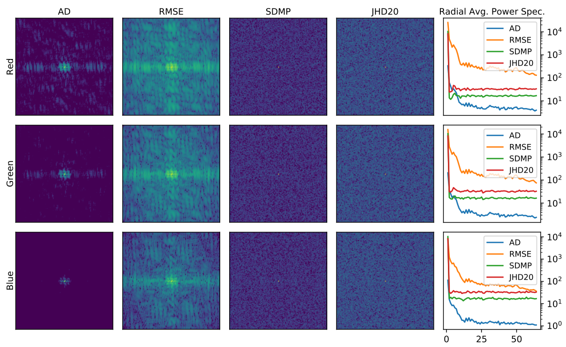

Figure 8: The fast Fourier transform (FFT) power spectra corresponding to the control images in Figure 4. The first four columns (from the left) show the 2D power spectra for each approach, while the rightmost column shows plots of the radially averaged power spectra. The rows correspond to the RGB channels. Here, we observe that our approach and JHD20, in contrast to the others, have a very uniform spectrum.This characteristic allows us to show biased regions clearly, without distracting scene features from unbiased regions.

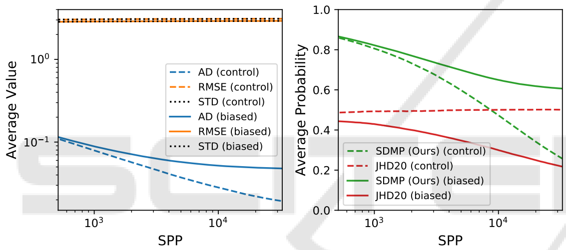

Figure 9: The average image values with respect to the number of SPP for the (unbiased) control and the biased renderings of all approaches shown in Figure 6. We note that higher values correspond to more difference, expect for JHD20. The latter is based on Welch's p-value, which, in the case of no difference, is 0.5 on average, and lower otherwise.

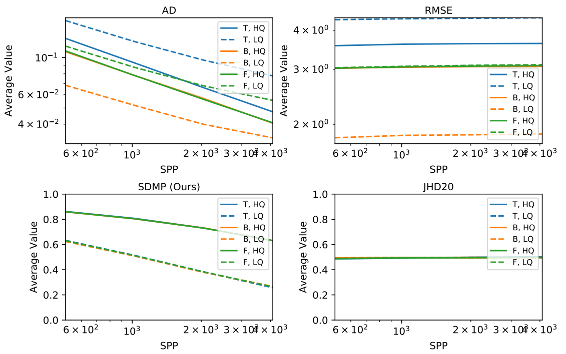

Figure 10: Plots showing the average values of the different measures aggregated over different images regions at specific sample counts. The values correspond to the control images shown in Figure 5. The image regions (T, B, F) are shown in Figure 12. The dashed lines correspond to a low-quality (LQ) reference ($n = 4,096$), and the solid lines correspond to a high-quality (HQ) reference ($n = 32,768$).

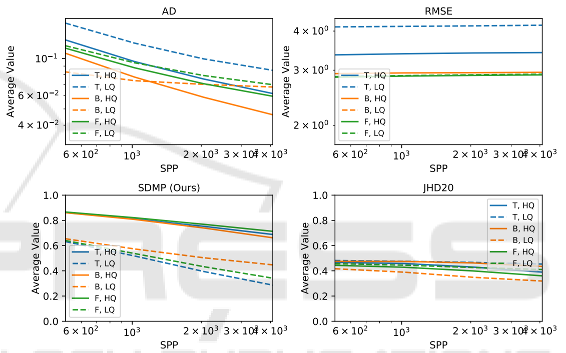

Figure 11: These plots are analogous to the ones shown in Figure 10 with the difference that they are computed for the biased case.

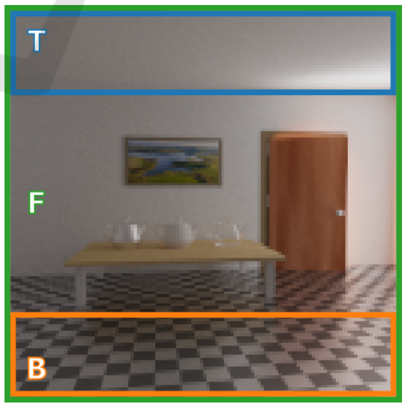

Figure 12: The image regions T (top), B (bottom), and F (full) corresponding to the average values reported in Figures 10 to 11.

proach, in contrast to the others, incorporates the accuracy of the reference.

In Figure 11, we show the plots corresponding to the biased renderings of the VEACH AJAR scene. In this case, the bottom region (orange) covers the biased values. We can see how the SDMP clearly indicates the differences between the regions in both the high and low-quality reference cases. This is less the case for JHD20 since the p-values do not incorporate the accuracy of the reference.

Implementation Details. For rendering, we have used Mitsuba (Jakob, 2010), which we have slightly modified to be able to set the seed of the random number generator (RNG). We chose the independent sampler and the box filter for all cases. In general, our approach can be used with any renderer for which the RNG seed can be specified. All necessary statistics for the SDMP can be calculated online, i.e. without maintaining individual samples (by e.g., using Welford's algorithm (Welford, 1962)). We choose $\alpha = 0.05$ for all experiments—a common choice for hypothesis testing. For the visualization of the rendered images, we chose the global tone mapper by Reinhard et al. (Reinhard et al., 2002), while the values of all other (non-radiance) images were clipped to their 0.95 percentile to mitigate outliers and normalized such that meaningful comparisons are possible.

5.2 Comparison to Jung et al.

In the following, we further investigate the differences of our approach to the closely related work by Jung et al. (Jung et al., 2020). Both approaches essentially build on the same statistical quantities for two independent sample sets. The main difference is that Welch's test, used by Jung et al., estimates the sampling distribution of the difference between means ($\bar{X}_n - \bar{Y}_n$) and computes the corresponding p-value. Our approach estimates the SDMs of both sample sets individually and computes the likelihood that one mean ($\bar{Y}_n$) takes on values inside the CI of the other mean ($\bar{X}_n$) (as described in Equation 7).

Therefore, both approaches compute probabilities that correspond to a form of difference. However, both probabilities exhibit different characteristics. In case of no bias, Welch's p-values are always uniformly distributed and therefore 0.5 on average, regardless of the error of the sample means. With increasing bias, the distribution of the p-values becomes skewed toward zero. By contrast, in case of no bias, the SDMP is not 0.5 on average but can take on any value between zero and one, thereby being free to indicate how similar the two SDMs are. This property can be seen in Figure 9. In the case of no bias, the p-value (JHD20; red dashed line) is constant, regardless of sample count. In contrast, our SDMP decreases with increased sample count, indicating the convergence of the unbiased control rendering toward the reference rendering. In case of bias, the p-value converges toward zero, whereas the SDMP converges toward a particular value, depending on the error of the reference.

Both approaches build on the central limit theorem (CLT) and assume normally distributed sample means. Jung et al. aggregate MC samples over image tiles to ensure normality. For our comparison we have not performed this aggregation but computed a high number of SPP instead. Figure 7 shows that outliers (e.g., due to fireflies) can violate the normality assumption. As already discussed by Jung et al., this can lead to undesired structure and wrong results in regions of such outliers. In order to investigate this issue, we have performed a simulation study using the Kolmogorov–Smirnov test for normality (summarized in Figure 13), which suggests that fireflies can indeed violate the normality assumption.

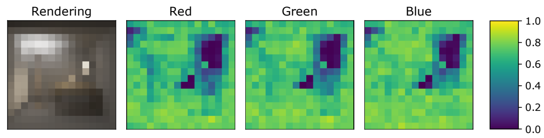

Figure 13: A rendering (left) of the VEACH BIDIR ROOM scene and the average p-values of the Kolmogorov–Smirnov test for normality of the radiance sample means for each color channel (three rightmost columns). We can see that for most regions of the rendering, the p-values are relatively high, suggesting normality. However, in some regions, fireflies (seen in Figure 7) skew the distribution of the mean. This results in low p-values which indicate a divergence from normality.

6 CONCLUSION

In this paper, we have discussed how sampling distribution of the mean (SDM)-based approaches can facilitate the per-pixel comparison of Monte Carlo (MC) renderings and techniques. While the absolute deviation (AD) can show differences, it tends to exhibit structured noise that makes it difficult to distinguish actual bias from variability. This is even more problematic for the root mean squared error (RMSE), since it is inherently tied to the variability of the integrator, which makes it difficult to detect bias that is smaller in comparison. The recent approach by Jung et al. (Jung et al., 2020) can detect bias at low sample counts. However, due to the properties of Welch's p-value, the approach is agnostic to the state of convergence of renderings. In contrast, our approach takes the state of convergence into account. Our results suggest that our approach is a promising alternative for the comparison and evaluation of MC renderings and techniques.

Limitations. Our approach, as well as that by Jung et al., builds on the assumption of normally distributed sample means. Therefore, measures to ensure normality should be applied, such as tiling or the use of higher sample counts.

ACKNOWLEDGMENTS

This research was funded by the Austrian Science Fund (FWF) through project ORD 61 "A Test Suite for Photorealistic Rendering and Filtering" and F 77 "Advanced Computational Design".

REFERENCES

Andersson, P., Nilsson, J., Akenine-Möller, T., Oskarsson, M., Åström, K., and Fairchild, M. D. (2020). ꟻLIP:

A Difference Evaluator for Alternating Images. *Proceedings of the ACM on Computer Graphics and Interactive Techniques*, 3(2):15:1–15:23.

Bärz, J., Henrich, N., and Müller, S. (2010). Validating photometric and colorimetric consistency of physically-based image synthesis. In *5th European Conference on Colour in Graphics, Imaging, and Vision and 12th International Symposium on Multispectral Colour Science, CGIV 2010/MCS'10, Joensuu, Finland, June 14-17, 2010*, pages 148–154. IS&T - The Society for Imaging Science and Technology.

Bitterli, B. (2016). Rendering resources. https://benedikt-bitterli.me/resources/.

Celarek, A., Jakob, W., Wimmer, M., and Lehtinen, J. (2019). Quantifying the error of light transport algorithms. *Comput. Graphics Forum*, 38(4):111–121.

Clausen, O., Marroquim, R., and Fuhrmann, A. (2018). Acquisition and validation of spectral ground truth data for predictive rendering of rough surfaces. In *Computer Graphics Forum*, volume 37, pages 1–12. Wiley Online Library.

Daly, S. (1993). Digital images and human vision. chapter The Visible Differences Predictor: An Algorithm for the Assessment of Image Fidelity, pages 179–206. MIT Press, Cambridge, MA, USA.

Farrugia, J.-P. and Péroche, B. (2004). A progressive rendering algorithm using an adaptive perceptually based image metric. *Comput. Graphics Forum*, 23(3):605–614.

Goral, C. M., Torrance, K. E., Greenberg, D. P., and Battaile, B. (1984). Modeling the interaction of light between diffuse surfaces. In *Proceedings of the 11th Annual Conference on Computer Graphics and Interactive Techniques*, SIGGRAPH '84, pages 213–222, New York, NY, USA. ACM.

Jakob, W. (2010). Mitsuba renderer. http://www.mitsuba-renderer.org.

Jones, N. L. and Reinhart, C. F. (2017). Experimental validation of ray tracing as a means of image-based visual discomfort prediction. *Build. Environ.*, 113:131–150. Advances in daylighting and visual comfort research.

Jung, A., Hanika, J., and Dachsbacher, C. (2020). Detecting bias in Monte Carlo renderers using Welch's t-test. *Journal of Computer Graphics Techniques (JCGT)*, 9(2):1–25.

Kajiya, J. T. (1986). The rendering equation. *SIGGRAPH Comput. Graph.*, 20(4):143–150.

Mantiuk, R., Daly, S. J., Myszkowski, K., and Seidel, H. (2005). Predicting visible differences in high dynamic range images: model and its calibration. In Rogowitz, B. E., Pappas, T. N., and Daly, S. J., editors, *Human Vision and Electronic Imaging X, San Jose, CA, USA, January 17, 2005*, volume 5666 of *SPIE Proceedings*, pages 204–214. SPIE.

Mantiuk, R., Kim, K. J., Rempel, A. G., and Heidrich, W. (2011). HDR-VDP-2: a calibrated visual metric for visibility and quality predictions in all luminance conditions. *ACM Trans. Graph.*, 30(4):40:1–40:14.

McNamara, A. (2006). Exploring visual and automatic measures of perceptual fidelity in real and simulated imagery. *ACM Trans. Appl. Percept.*, 3(3):217–238.

McNamara, A., Chalmers, A., Troscianko, T., and Gilchrist, I. (2000). Comparing real & synthetic scenes using human judgements of lightness. In Péroche, B. and Rushmeier, H., editors, *Rendering Techniques 2000*, pages 207–218, Vienna. Springer Vienna.

Meneghel, G. B. and Netto, M. L. (2015). A comparison of global illumination methods using perceptual quality metrics. In *2015 28th SIBGRAPI Conference on Graphics, Patterns and Images*, pages 33–40.

Meseth, J., Müller, G., Klein, R., Röder, F., and Arnold, M. (2006). Verification of rendering quality from measured BTFs. In *Proceedings of the 3rd Symposium on Applied Perception in Graphics and Visualization*, APGV '06, page 127–134, New York, NY, USA. Association for Computing Machinery.

Myszkowski, K. (1998). The visible differences predictor: Applications to global illumination problems. In *Rendering Techniques*.

Narwaria, M., Mantiuk, R. K., Da Silva, M. P., and Le Callet, P. (2015). HDR-VDP-2.2: a calibrated method for objective quality prediction of high-dynamic range and standard images. *J. Electron. Imaging*, 24(1):010501–010501.

Pattanaik, S. N., Ferwerda, J. A., Fairchild, M. D., and Greenberg, D. P. (1998). A multiscale model of adaptation and spatial vision for realistic image display. In Cunningham, S., Bransford, W., and Cohen, M. F., editors, *Proceedings of the 25th Annual Conference on Computer Graphics and Interactive Techniques, SIGGRAPH 1998, Orlando, FL, USA, July 19-24, 1998*, pages 287–298. ACM.

Ramasubramanian, M., Pattanaik, S. N., and Greenberg, D. P. (1999). A perceptually based physical error metric for realistic image synthesis. In *Proceedings of the 26th Annual Conference on Computer Graphics and Interactive Techniques*, SIGGRAPH '99, pages 73–82, New York, NY, USA. ACM Press/Addison-Wesley Publishing Co.

Reinhard, E., Stark, M., Shirley, P., and Ferwerda, J. (2002). Photographic tone reproduction for digital images. *ACM Trans. Graph.*, 21(3):267–276.

Schregle, R. and Wienold, J. (2004). Physical validation of global illumination methods: Measurement and error analysis. *Comput. Graphics Forum*, 23(4):761–781.

Subr, K. and Arvo, J. (2007). Statistical hypothesis testing for assessing Monte Carlo estimators: Applications to image synthesis. In *Computer Graphics and Applications, 2007. PG'07. 15th Pacific Conference on*, pages 106–115. IEEE.

Ulbricht, C., Wilkie, A., and Purgathofer, W. (2006). Verification of physically based rendering algorithms. *Comput. Graphics Forum*, 25(2):237–255.

Volevich, V., Myszkowski, K., Khodulev, A., and Kopylov, E. A. (2000). Using the visual differences predictor to improve performance of progressive global illumination computation. *ACM Trans. Graph.*, 19(2):122–161.

Wang, Z., Bovik, A. C., Sheikh, H. R., and Simoncelli, E. P. (2004). Image quality assessment: from error visibility to structural similarity. *IEEE Trans. Image Processing*, 13(4):600–612.

Welford, B. P. (1962). Note on a method for calculating corrected sums of squares and products. *Technometrics*, 4(3):419–420.

Whittle, J., Jones, M. W., and Mantiuk, R. (2017). Analysis of reported error in Monte Carlo rendered images. *The Visual Computer*, 33(6):705–713.